Research Article Open Access

Maha S. Almutairi, S. Soumya, Reem I. Al-Wabli, I. Hubert Joe, Mohamed I. Attia*

Density functional theory calculations, vibration spectral analysis and molecular docking of the antimicrobial agent 6-(1,3-benzodioxol-5-ylmethyl)-5-ethyl-2-{[2-(morpholin-4-yl)ethyl] sulfanyl}pyrimidin-4(3*H*)-one

https://doi.org/10.1515/chem-2018-0067 received January 14, 2018; accepted April 13, 2018.

Abstract: Vibrational spectral analysis and quantum chemical computations based on density functional theory have been performed on the antimicrobial agent 6-(1,3-benzodioxol-5-ylmethyl)-5-ethyl-2-{[2-(morpholin-4-yl)ethyl]sulfanyl}pyrimidin-4-(3*H*)-one. The equilibrium structural geometry, various bonding features and harmonic vibrational wavenumbers of the title compound have been investigated using DFT-B3LYP function at 6-311++G(d,p) basis set. The detailed interpretations of the vibrational spectra have been carried out with the aid of VEDA 4 program. The various intramolecular interactions of the title compound have been exposed by natural bond orbital analysis. The FT-IR and FT-Raman spectra of the title molecule have been recorded and analyzed. Blueshifting of the C-H wavenumber along with a decrease in the C-H bond length attribute for the formation of the C-H...O hydrogen bonding provide an evidence for a charge transfer interaction. Also, the distribution of natural atomic charges reflects the presence of intramolecular hydrogen bonding. The analysis of the electron density of HOMO and LUMO gives an idea of the delocalization and

the low value of energy gap indicates electron transfer within the molecule. Moreover, molecular docking studies revealed the possible binding of the title molecule to different antimicrobial target proteins.

Keywords: Pyrimidinones; Thiouracils; DFT; Molecular docking; HOMO-LUMO.

1 Introduction

Heterocyclic compounds bearing nitrogen atoms in their structural skeletons are found in many biologically active natural products and display appreciable therapeutic applications: among them, pyrimidines which constitute eminent parts in the chemistry of nucleic acids [1]. The pyrimidine system constitutes the key pharmacophore of several non-nucleoside chemotherapeutic agents due to their ability to inhibit vital enzymes responsible for DNA biosynthesis, such as dihydrofolate reductase, thymidylate synthetase, thymidine phosphorylase and reverse transcriptase [2]. In addition, the multi-functionalized pyrimidines exhibit diverse pharmacological efficiencies including anticancer [3-5], antiviral [6], antitubercular [7], antibacterial [8], anti-fungal [9] and anti-inflammatory [10] activities. Uracils are pyrimidine derivatives which are considered as privileged structures in drug innovation process due to their wide spectrum of biological activities, synthetic accessibility and ability to give drug like properties [11-13].

On the other hand, a number of biologically active molecules have the 1,3-benzodioxole fragment in their chemical skeletons and they display a wide array of biological activities such as anticancer [14], antioxidant

^{*}Corresponding author: Mohamed I. Attia, Department of Pharmaceutical Chemistry, College of Pharmacy, King Saud University, P.O. Box 2457, Riyadh 11451, Saudi Arabia; Medicinal and Pharmaceutical Chemistry Department, Pharmaceutical and Drug Industries Research Division, National Research Centre (ID: 60014618), El Bohooth Street, Dokki, Giza 12622, Egypt, E-mail: mattia@ksu.edu.sa Maha S. Almutairi, Reem I. Al-Wabli: Department of Pharmaceutical Chemistry, College of Pharmacy, King Saud University, P.O. Box 2457, Riyadh 11451, Saudi Arabia

S. Soumya, I. Hubert Joe: Centre for Molecular and Biophysics Research, Department of Physics, Mar Ivanios College(Autonomous), Thiruvananthapuram-695 015, Kerala, India

[15], antiprotozoal [16] and immunomodulatory [17] activities.

Molecular hybridization is a well documented effective strategy in synthetic medicinal chemistry to get bioactive new chemical entities [18]. Covalent combination of two or more drug pharmacophores into a single molecule gave molecular hybrids which might devoid of unwanted side effects with concomitant synergic effect and better activity in many cases [19].

Molecular hybridization of thiouracil nucleus and 1,3-benzodioxole fragment furnished the title compound 6-(1,3-benzodioxol-5-ylmethyl)-5-ethyl-2-{[2-(morpholin-4-yl)ethyl]sulfanyl}pyrimidin-4(3H)-one which displayed antimicrobial activity against *Bacillus subtilis*, *Bacillus cereus* and *Aspergillus niger* with minimum inhibitory concentration (MIC) value of 0.19 μ mol/mL [20]. Therefore, we were encouraged to carry out the current spectroscopic characterization and density functional theory (DFT) computations on the title compound aiming to get more insights into its electronic properties as well as its natural charge distribution which might influence the interaction with its target protein. Moreover, molecular docking studies explored the possible binding mode of the title compound to its target protein.

2 Materials and methods

2.1 General

The FT-Raman spectrum of the title compound was carried out on a Bruker RFS-27 FT-Raman spectrometer (Bruker, Billerica, MA, USA) in the region 4000-50 cm⁻¹. The 1064 nm line of Nd:YAG laser operating at 100 mW power was used for excitation and the spectral resolution was 2 cm⁻¹. The FT-IR spectrum of the title compound was recorded in the 4000-400 cm⁻¹ range using a Perkin Elmer RXL spectrophotometer (Perkin-Elmer, Ayer Rajah Crescent Level, Singapore), with sample in KBr using pellet press method. The spectral resolution was 1 cm⁻¹.

2.2 Synthesis

The title compound molecule was prepared as previously reported in the literature [20].

2.3 Computational details

All DFT computations of the title compound have been performed using Gaussian '09 [21] program package at the Becke3-Lee-Yang-Parr (B3LYP) level with 6-311++G(d,p) basis set [22-25]. In order to correct the over-estimations arising from some negative factors such as basis set incompleteness and anharmonicity characters of the vibrational modes, the calculated wavenumbers were scaled using a uniform scaling factor of 0.9673 [26]. The distributions of assignment of the calculated wavenumbers were aided by VEDA4 program [27]. Natural charge analyses along with HOMO-LUMO have been used to elucidate information regarding charge transfer within the molecule. The Raman activities (S_i) calculated in the harmonic frequency calculations were later converted to relative Raman intensities (I) using the following relationship derived from the basic theory of Raman scattering [28].

$$I_i = \frac{f(v_0 - v_i)^4 S_i}{v_i \left[1 - exp\left(\frac{-hcv_i}{kT}\right) \right]} \tag{1}$$

where v_0 is the exciting wavenumber (in cm⁻¹), v_i is the vibrational wavenumber of the ith normal mode, h, c and k are the universal constants and 'f' is a suitably chosen common scaling factor for all the peak intensities. The simulated IR and Raman spectra were plotted using pure Lorentzian band shapes with a full width half maximum (FWHM) of 10 cm⁻¹.

Ethical approval: The conducted research is not related to either human or animals use.

3 Results and Discussion

3.1 Synthesis

The title compound was prepared as depicted in Schemes 1 and 2 by adopting the reported procedure [20]. The spectral data of the title molecule were in agreement with the reported ones [29].

3.2 Optimized geometry

The optimized molecular structure of 6-(1,3-benzodioxol-5-ylmethyl)-5-ethyl-2-{[2-(morpholin-4-yl)ethyl] sulfanylpyrimidin-4(3*H*)-one obtained from DFT

Reagents and conditions: i) NaBH $_{\!_4}$, methanol, RT, 18 h; ii) SOCl $_{\!_2}$, RT, 18 h; iii) NaCN, KI, DMF, RT, 18 h

Scheme 1: Preparation of the intermediate compound 4.

Reagents and conditions: i) (1) Zn/THF (2) K_2CO_3 (3) HCl; ii) (1) NH_2CSNH_2 , NaOEt, ethanol, reflux, 24 h (2) HCl; iii) N-(2-chloroethyl) morpholine hydrochloride, K_2CO_3 , DMF, RT, 18 h.

Scheme 2: Preparation of the title molecule 8.

calculations at B3LYP level with 6-311++G(d,p) basis set is shown in Figure 1 and the geometrical parameters obtained from optimized geometry and XRD data are presented in Table 1. The asymmetry of the benzene ring is evident from the negative deviation in the bond angles of C36-C35-C34 and C37-C38-C39 as well as the positive deviation of the remaining angles from the normal value of 120°, which might be attributed to the presence of 1,3-dioxolane group. The interesting structural features of the title compound are the decrease of the cyclic angles C36-C35-C34 and C37-C38-C39 along with the increase of the neighbouring angles around the ring indicating a charge transfer (CT) interaction in the 1,3-benzodioxole moiety. Similarly, the decrease of the bond angle of C39-C34-C35 by ~3.4° and the increase of the bond angle of C34-C39-C38 by ~2.42° is associated with CT interaction between the 1,3-benzodioxole and pyrimidinone groups. The DFT calculations also gave a decrease in the bond angle of C31-C34-C35 by 0.35° and an increase in the bond angle of C31-C34-C39 by 0.75° from 120° at C34 position. This asymmetry of exocyclic angles reveals the repulsion between the CH, group and the phenyl ring. Hyperconjugation of the carbonyl group with the adjacent C18-C19 single bond, which is evident from the bond distance of 1.22 and 1.46 Å for C18=O23 and C18-C19, respectively.

The contraction of the C1-H8 bond length (1.091 Å) from the other methylene C-H bonds and the H8....042

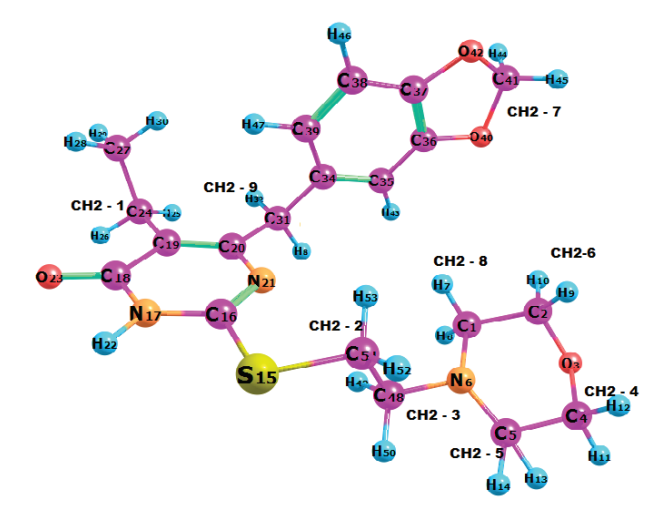
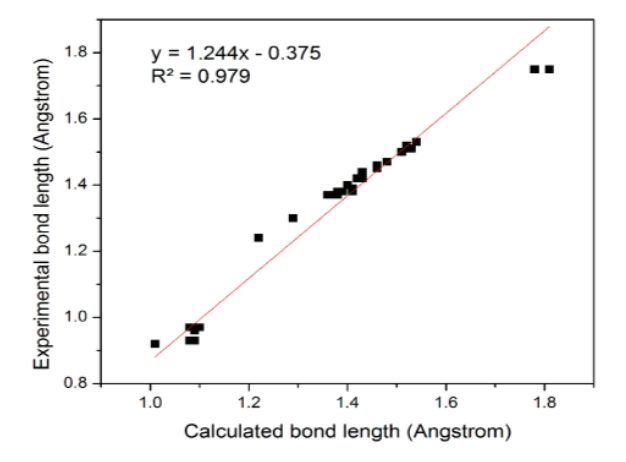


Figure 1: The optimized molecular structure of the title molecule based on the B3LYP/6-311++G(d,p) level of basis set.



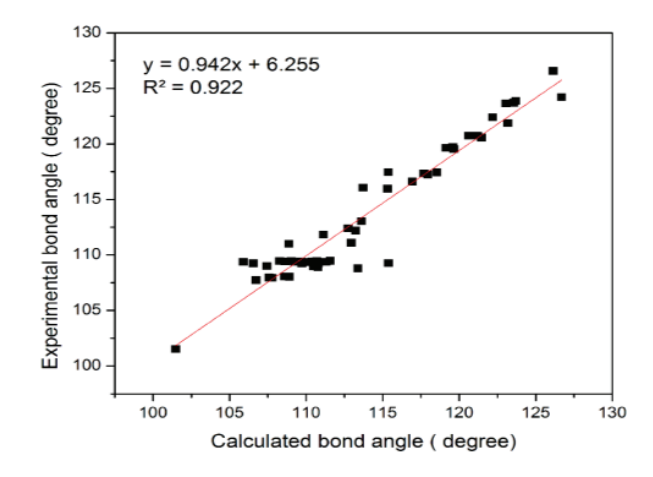


Figure 2: Linear curve fitting plots of the calculated and experimental bond lengths and bond angles parameters for the title compound.

Table 1: The calculated optimized geometrical parameters of compound at B3LYP/6-311++G(d,p) level of basis set.

Bond length	Calc. (Å)	Expt. (Å)	Bond angle	Calc. (°)	Expt. (°)	Torsion angle	Calc. (°)	Expt. (°)
C1-C2	1.54	1.51	C2-C1-N6	108.64	111.34	N6-C1-C2-O3	39.29	-58.69
C1-N6	1.47	1.46	C 2-C1-H7	109.07	109.31	N6-C1-C2-H9	161.58	179.61
C1-H7	1.09	0.97	C2-C1-H8	111.59	109.31	N6-C1-C2-H10	-79.07	62.19
C1-H8	1.10	0.97	N6-C1-H7	108.62	109.43	H7-C1-C2-O3	157.52	62.33
C2-03	1.43	1.43	N6-C1-H8	111.29	109.39	H7-C1-C2-H9	-80.18	-58.79
C2-H9	1.10	0.97	H7-C1-H8	107.58	107.98	H7-C1-C2-H10	39.16	59.40
C2-H10	1.09	0.97	C1-C2-O3	112.94	111.11	H8-C1-C2-O3	-83.77	-179.67
O3-C4	1.42	1.42	C1-C2-H9	109.24	109.39	H8-C1-C2-H9	38.53	59.40
C4-C5	1.53	1.51	C1-C2-H10	110.41	109.40	H8-C1-C2-H10	157.87	-58.79
C4-H11	1.10	0.97	03-C2-H9	109.64	109.43	C2-C1-N6-C5	-58.27	54.39
C4-H12	1.09	0.97	03-C2-H10	105.90	109.38	H7-C1-N6-C5	-176.78	-66.56
C5-N6	1.48	1.47	H9-C2-H10	108.59	108.07	C1-C2-O3-C4	19.51	59.80
C5-H13	1.09	0.97	C2-03-C4	113.39	108.80	H9-C2-O3-C4	-102.56	-170.34
C5-H14	1.10	0.97	03-C4-C5	111.13	111.84	H10-C2-O3-C4	140.47	-61.08
S15-C16	1.78	1.75	03-C4-H11	110.80	109.25	C2-03-C4-C5	-64.03	-59.41
S15-C16	1.81	1.75	03-C4-H12	106.56	109.26	C2-03-C4-H12	176.48	179.52
C16-N17	1.36	1.37	C5-C4-H11	110.70	109.45	03-C4-C5-N6	43.98	57.39
C16-N21	1.29	1.30	C5-C4-H12	109.72	109.24	03-C4-C5-H13	-74.60	-63.52
N17-C18	1.41	1.38	H11-C4-H12	107.79	107.96	03-C4-C5-H14	165.94	178.28
N17-H22	1.01	0.92	C4-C5-N6	108.89	110.99	H11-C4-C5-N6	-79.60	-63.66
C18-C19	1.46	1.45	C 4-C5-H13	110.13	109.37	H11-C4-C5-H13	161.83	175.43
C18-O23	1.22	1.24	C4-C5-H14	109.04	109.45	H11-C4-C5-H14	42.36	57.23
C19-C20	1.37	1.37	N6-C5-H13	108.27	109.45	H12-C4-C5-N6	161.57	178.48
C19-C24	1.51	1.50	N6-C5-H14	111.58	109.47	H12-C4-C5-H13	42.99	57.57
C20-N21	1.38	1.38	H13-C5-H14	108.92	108.05	H12-C4-C5-H14	-76.48	-60.64
C20-C31	1.52	1.51	C1-N6-C5	115.38	109.27	C4-C5-N6-C1	16.74	-53.38
C24-H25	1.09	0.97	N6-C48-H49	110.77	108.91	H13-C5-N6-C1	136.49	67.53
C24-H26	1.09	0.97	C48-C51-S15	113.23	112.18	H14-C5-N6-C1	-103.66	-174.21
C24-C27	1.54	1.53	C51-S15-C16	101.48	101.53	S15-C16-N17-C18	-179.60	178.67
C27-H28	1.09	0.96	N17-C16-N21	123.06	123.63	S15-C16-N17-H22	0.23	4.48
C27-H29	1.09	0.96	C16-N17-C18	123.17	121.88	N21-C16-N17-C18	0.59	1.81
C27-H30	1.09	0.96	C16-N17-H22	121.45	120.58	N21-C16-N17-H22	-179.58	-175.04
C31-H32	1.09	0.97	C18-N17-H22	115.37	117.47	S15-C16-N21-C20	-179.53	179.24
C31-H33	1.10	0.97	N17-C18-C19	113.72	116.05	N17-C16-N21-C20	0.26	-1.28
C31-C34	1.52	1.52	N17-C18-O23	119.58	119.72	C16-N17-C18-C19	-0.28	-0.46

Continued Table 1: The calculated optimized geometrical parameters of compound at B3LYP/6-311++G(d,p) level of basis set.

Bond length	Calc. (Å)	Expt. (Å)	Bond angle	Calc. (°)	Expt. (°)	Torsion angle	Calc. (°)	Expt.
C34-C35	1.41	1.39	C19-C18-O23	126.70	124.23	C16-N17-C18-O23	179.72	179.66
C34-C39	1.40	1.40	C18-C19-C20	118.54	117.45	H22-N17-C18-C19	179.88	176.48
C35-C36	1.38	1.37	C18-C19-C24	115.32	115.97	H22-N17-C18-O23	-0.12	-3.39
C35-H43	1.08	0.93	C20-C19-C24	126.14	126.57	N17-C18-C19-C24	179.41	179.68
C36-C37	1.39	1.38	C19-C20-N21	123.55	123.72	023-C18-C19-C24	-0.59	-0.45
C36-040	1.38	1.38	C19-C20-C31	123.69	123.87	C18-C19-C20-C31	-179.14	-177.96
C37-C38	1.38	1.37	N21-C20-C31	112.75	112.41	C24-C19-C20-C31	0.58	1.05
C37-042	1.38	1.38	C16-N21-C20	117.94	117.24	C18-C19-C24-C27	82.60	74.61
C38-C39	1.40	1.40	C19-C24-H25	107.44	109.00	C20-C19-C24-C27	-97.13	-104.42
C38-H46	1.08	0.93	C19-C24-H26	110.50	108.96	C19-C20-C31-C34	125.59	-11.61
C39-H47	1.08	0.93	C19-C24-C27	113.62	113.05	N21-C20-C31-C34	-55.23	-69.92
040-C41	1.43	1.44	H25-C24-H26	106.72	107.73	C20-C31-C34-C39	-58.13	109.14
C41-O42	1.43	1.42	C31-C34-C35	119.12	119.65	H32-C31-C34-C35	-112.75	-129.46
C41-H44	1.09	0.97	C31-C34-H39	121.20	120.75	C31-C34-C35-C36	178.35	175.81
N6-C48	1.46	1.46	C39-C34-C35	119.64	119.54	C31-C34-C35-H43	-1.68	-4.19
C48-H50	1.10	0.97	C31-C34-C39	120.63	120.75	H43-C35-C36-C37	-179.60	-179.26
C48-H49	1.09	0.97	C34-C39-C38	122.19	122.42	C35-C36-C37-O42	177.61	178.27
C51-H52	1.09	0.97	C34-C35-C36	117.70	117.36	040-C36-C37-C38	-177.75	179.17
C5-H53	1.09	0.97	C37-C38-C39	116.94	116.60	H44-C41-O42-C37	-138.76	-116.63

bond distance of 2.59 Å, which is shorter than the van der Waals radii of 2.72 [30], indicate C-H...O hydrogen bonding. Similarly C41-H45 bond length (1.083 Å) is much shorter than any other C-H bonds. H45.....040 bond length is only 2.012 Å, which is shorter than van der Waals radii, indicating hydrogen bonding. The hydrogen bridge tends to push the two hetero atoms closer to each other.

The linear fitting graphs (Figure 2) manifested the correlation between the experimental and computed results. The correlation between the calculated and experimental bond lengths and bond angles showed R^2 values of 0.979 and 0.922, respectively. The statistical results revealed that the computed results are in good agreement with the experimental XRD values. Therefore, this computation method was considered to carry out the required vibrational studies, natural bond orbital and Frontier orbital energy analyses.

3.3 Natural bond orbital analysis

The natural bond orbital (NBO) analysis is proved to be an effective tool for chemical interpretation of hyperconjugative interactions and electron density transfer (EDT) from filled lone electron pairs of the n(Y) of the "Lewis base" Y into the unfilled anti bond $\sigma^*(X-H)$ of the "Lewis acid" X-H in X-H---Y hydrogen bonding systems [30]. NBO analysis provides a description of the structure of a conformer by a set of localized bonds, antibonds and Rydberg extra valence orbitals. Stabilizing interactions between the filled and unoccupied orbitals and destabilizing interactions between the filled orbitals can also be obtained from this analysis [31]. The lowering of orbital energy due to the interaction between the doubly occupied orbital and the unoccupied ones is a very convenient guide to interpret the molecular structure. In energetic terms, hyperconjugation is an important effect [32] in which an occupied Lewis-type natural bond orbital

Table 2: The most important interactions between 'filled' (donors) Lewis-type NBOs and 'empty' (acceptors) non-Lewis NBOs of the title compound.

Donor (i)	ED (i)e	Acceptor (j)	ED (j)e	E(2) ^a (kcal/mol)	E(j)-E(i) ^b (a.u.)	F(i,j) ^c (a.u.)
π (C19-C20)	1.77576	π*(C16-N21)	0.36608	10.20	0.26	0.048
π (C19-C20)	1.77576	π*(C18-O23)	0.34349	25.90	0.28	0.079
n1 (03)	1.96421	σ* (C4-H12)	0.01402	2.48	0.96	0.044
n2 (03)	1.92515	σ*(C4-C5)	0.02547	6.13	0.66	0.057
n2 (03)	1.92515	σ*(C4-H11)	0.03004	5.83	0.67	0.057
n1 (N17)	1.60742	σ*(C16-N21)	0.01966	58.60	0.28	0.114
n1 (N17)	1.60742	σ*(C18-O23)	0.00967	46.00	0.30	0.106
n1 (023)	1.97888	σ*(N17-C18)	0.09184	1.02	1.07	0.030
n1 (023)	1.97888	σ*(C18-C19)	0.06139	2.71	1.15	0.050
n2 (023)	1.85977	σ*(N17-C18)	0.09184	29.10	0.64	0.123
n2 (023)	1.85977	π*(C18-C19)	0.06139	16.60	0.72	0.100
n2 (040)	1.86172	σ* (C35-C36)	0.37937	25.30	0.35	0.090
n2 (040)	1.86172	σ*(C41-H45)	0.03860	6.14	0.68	0.059
n2 (042)	1.86390	π* (C37-C38)	0.37833	24.90	0.35	0.089
n2 (042)	1.86390	σ* (C41-H45)	0.03860	6.22	0.68	0.060

^a Energy of hyperconjugative interactions; ^b Energy difference between donor and acceptor i and j NBO orbitals; ^c The Fock matrix element between i and j NBO orbitals.

is stabilized by overlapping with a non Lewis-type orbital (either one-center Rydberg or two-center antibonding NBO). This electron delocalization can be described as a charge transfer from a Lewis valence orbital (donor), with a decreasing of its occupancy, to a non-Lewis orbital (acceptor). Several other types of valuable data, such as directionality, hybridization and partial charges, were analyzed in the output of NBO analysis. The second-order perturbation theory analysis of Fock matrix in the NBO of the title compound shows strong intramolecular hyperconjugative interactions, which are presented in Table 2.

The intramolecular hyperconjugative interactions are formed by the orbital overlap between $\pi^*(C-C)$ and $\pi^{\star}(\text{C-C})$ bond orbitals which results in an intramolecular charge transfer (ICT) causing stabilization of the system [33]. These interactions are observed as an increase in the electron density (ED) in C19-C20 anti-bonding orbital that weakens the respective bonds. The strong intramolecular hyperconjugative interaction of π electrons from C16-N21 bond to the π^* (C19-C20) bond of pyrimidine ring increases ED. Similar effect is shown by π (C19-C20) to π *(C18-O23). Energy E(2)associated with hyperconjugative interactions $n2(O3)\rightarrow\sigma^*(C4-H11)$, $n2(O3)\rightarrow\sigma^*(C4-H12)$,

 $n2(O42)\rightarrow\sigma^*(C41\text{-H}45)$ and $n2(O40)\rightarrow\sigma^*(C41\text{-H}45)$ are obtained as 5.83, 2.48, 6.22 ,6.14 kcal.mol⁻¹, respectively which quantify the extend of intramolecular hydrogen bonding.

The differences in E(2) energies are reasonably due to the fact that the accumulation of electron density in the C-H bond is not only drawn from the n(O) of hydrogenacceptor but also from the entire molecule. The orbital interaction energy for n2(O23) \rightarrow σ^* (C18-C19) is 16.6 kcal. mol^{-1} and $\text{n1}(O23) \rightarrow \sigma^*(\text{N17-C18})$ is 29.1 kcal.mol⁻¹ which are higher values than the other delocalizations. This interaction is responsible for a pronounced increase of the O23 (1.97888e) orbital occupancy than the other occupancies, and it is possibly due to hyperconjugation between O23 and the pyrimidine ring. These ICTs around the rings can induce large bioactivity in the molecule. The *p*-character of the oxygen lone pair orbitals n2(O23) and n1(O23) is 99.89% and 40.34%, respectively, which is a very close to pure π -type lone pair orbital participates in electron donation to the $\sigma^*(C-O)$ orbital for the n1(N17) $\rightarrow \sigma^*$ (C18-O23) interaction in the title molecule. Also, an intermolecular hyperconjugative interaction occurs in $n2(S15) \rightarrow \sigma^*(C16-N21)$ which increases ED (0.01966e) that weakens the respective bond leading to stabilization of 23 kcal.mol⁻¹. The $n1(N17)\rightarrow \sigma^*(C16-N21)$ interaction shows the highest E(2) energy of 58.6 kcal.mol⁻¹.

3.4 Natural population analysis

Natural population analysis provides an effective method to calculate atomic charges and electron distribution within the molecule [34]. The net atomic charges of the title molecule, obtained by means of natural population analysis [35], are plotted in Figure 3. Very similar negative charges are noticed for the two oxygen atoms of the 1,3-benzodioxole group. A little more complicated situation is observed when the charges on the carbon atoms are considered. All hydrogen atoms have net positive charges and H22 (0.2073 e) shows more positive charge than the other hydrogen atoms due to its attachment with a nitrogen atom and with the oxygen atom of the pyrimidine ring N-H· · · O via intramolecular hydrogen bonding. All carbon atoms are negatively charged except C5, C16, C18, C20, C36, C37 and C41 due to their attachments with electronegative nitrogen, sulphur or oxygen atoms.

3.5 Vibrational analysis

The vibrational spectral analysis of the title compound has been performed based on the characteristic vibrations of its carbonyl, methylene, methyl and N-H groups. The computed vibrational wavenumbers, their IR and Raman activities as well as the atomic displacements corresponding to the different normal modes are used to identify the vibrational modes unambiguously. The selected vibrational assignments are presented in Table 3. The experimental and simulated FT-IR and FT-Raman spectra of the title compound are given in Figures 4 and 5, respectively. Correlation graphs between theoretical and experimental wavenumbers are given in Figure 6. There is a good agreement between the calculated and experimental values with a correlation coefficient (R^2) values = 0.999 for both IR and Raman.

3.5.1 Methyl group vibrations

Methyl groups are generally referred to as electron donating substituents in the aromatic ring systems. The methyl hydrogen atoms in the molecule are simultaneously subjected to hyperconjugation and back donation, which cause the decrease of stretching wavenumbers and IR

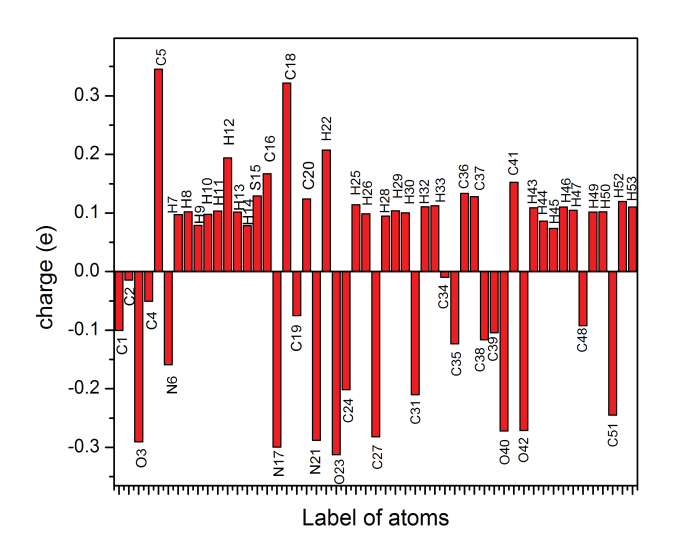


Figure 3: Natural charge distribution chart of the title molecule.

intensities [36]. Symmetric methyl stretching vibrations are normally observed between the wavenumbers 2952 and 2972 cm⁻¹, while the asymmetric stretching usually occurs between 2862 and 2882 cm⁻¹, respectively [37]. The methyl asymmetric stretching vibration of the title compound appears at 2973 cm⁻¹ as strong band in its FT-Raman spectrum, whereas its symmetric methyl stretching mode is observed at 2928 cm⁻¹ in its FT-IR spectrum. The increase in wavenumber by 91 cm⁻¹ (blue shifting) suggests the presence of intermolecular hydrogen bonding.

The asymmetrical bending vibrations usually occur in the range of 1450-1470 cm⁻¹, while the symmetrical bending vibrations appear in the range of 1365-1385 cm⁻¹ [33, 38]. The asymmetrical methyl vibrations generally overlap with the scissoring vibrations of the methylene groups. The asymmetrical bending vibrations of the title compound were identified at 1439 cm⁻¹ as medium FT-IR band and at 1441 cm⁻¹ as medium FT-Raman band. The absorption band arising from the symmetrical bending of the C-H bonds is very stable in position when the methyl group is attached to another carbon atom.

The rocking mode of the methyl group usually appears in the region of 1070-1010 cm¹ [35] and it is observed at 1361 cm⁻¹ as very weak band in the FT-IR spectrum of the title compound. Its methyl wagging vibrations occurred at 736 cm⁻¹ as weak bands in its FT-Raman spectrum.

3.5.2 Methylene group vibrations

The asymmetrical stretching and symmetrical stretching bands of the methylene groups occur near 2926 and 2855 cm⁻¹, respectively [39]. The wavenumber of the methylene stretching is increased when the methylene group is a part of a strained ring. The qualitative interpretation of intensities must rely on the understanding of some basic aspects of intramolecular charge distribution and on their effects on the IR intensities. The title compound has nine methylene groups. The $\mathrm{CH_2}(1)$ and $\mathrm{CH_2}(2)$ asymmetric stretching modes manifest their characteristic bands at 2967 and 2973 cm⁻¹ as a weak and strong bands in the FT-IR and FT-Raman spectra of the title compound, respectively. $\mathrm{CH_2}(3)$ symmetric stretching band occurs at 2916 cm⁻¹ in the FT-IR spectrum of the title compound as strong band and at 2922 cm⁻¹ in its FT-Raman spectrum as a very strong band.

CH₃(4) and CH₂(7) show a medium symmetric stretching band at 2875 cm⁻¹ in the FT-Raman spectrum with a blue shifting of 20 cm⁻¹ along with increase in the wavenumber of bending vibration by 18 cm⁻¹ indicating the possibility of C41-H45...O42 intramolecular hydrogen bond. This possibility can be confirmed from the optimized geometry and NBO analysis of the title compound. CH₂(8) symmetric stretching mode occurs as a weak band at 2933 cm⁻¹ Electronic effects including back-donation can shift the position and alter the intensity of methylene vibrations. The blue-shifting of the methylene stretching wavenumbers, point out to the influence of backdonation in the ring. The spectral analysis reveals that the methylene symmetric stretching modes are shifted to higher wavenumbers, probably because of electronic effects resulting from the influence of the methylene group on its adjacent groups.

The scissoring bands in the FT-IR spectra of hydrocarbons occur nearly at constant positions near 1465 cm⁻¹. The scissoring modes of methylene groups of the title compound are observed as strong band at 1483 cm⁻¹ in its FT-IR spectrum and as medium bands at 1441 and 1439 cm⁻¹ in the FT-Raman and FT-IR spectra, respectively. Moreover, the vibrational bands corresponding to the twisting, wagging, and rocking vibrations of the methylene groups and the in-plane and out-of plane deformation modes have also been observed and supported by DFT computations.

3.5.3 Carbonyl group vibrations

The intensity of carbonyl group bands can increase due to the conjugation or formation of hydrogen bonds. The carbonyl stretching vibrations in aromatic compounds are expected in the region of 1700-1640 cm⁻¹ [40].

The carbon-oxygen double bond is formed by π - π bond between carbon and oxygen and the lone pair of

electrons on the oxygen atom affects the nature of carbonyl group. A very weak carbonyl stretching band is formed at 1645 cm⁻¹ in the FT-Raman spectrum and at 1650 cm⁻¹ in the FT-IR spectrum of the title compound. NCO rocking is identified as weak bands in the FT-Raman spectrum of the title molecule at 558 cm⁻¹.

3.5.4 Aromatic CH vibration

Aromatic CH vibrations occur above 3000 cm 1 [40]. A very strong FT-IR band is noted at 3129 cm 1 and a very weak FT-Raman band at 3198 cm 1 corresponding to the aromatic CH stretching. FT-Raman weak bands are also found at 3106, 3066 and 3016 cm 1 . The intensity enhancement of C-H stretching wavenumber and decrease in intensity of the C-H bending wavenumber could be attributed to the conjugation with ring π system.

3.5.5 NH vibrations

The N-H stretching vibrations generally occur in the region of 3500-3300 cm $^{\scriptscriptstyle 1}$ [40]. The FT-IR band appeared at 3464 cm $^{\scriptscriptstyle 1}$ has been assigned to N-H stretching vibration. The red shifting is further enhanced by the reduction in the NH bond order values due to donor-acceptor interaction. The N-H in-plane bending mode is observed as a medium band in the FT-IR spectrum at 1497 cm $^{\scriptscriptstyle 1}$ and as a weak band at 1511 cm $^{\scriptscriptstyle 1}$ in FT-Raman spectrum.

3.5.6 C-S vibrations

The FT-IR stretching mode of the C-S bond usually occurs at 696 and 671 cm⁻¹ and Kaur et al. [41] reported that the C-S stretching mode appeared at 672 cm⁻¹. In the title compound, the C-S stretching band is observed at 466 cm⁻¹ in FT-IR spectrum as a medium band.

3.5.7 C-N and C-C vibrations

The C-N stretching vibrations generally occur in the region of 1350-1250 cm⁻¹. Symmetric stretching of C16-N17 and C18-N17 shows a weak band in the FT-Raman at 1135 cm⁻¹. Similarly, C1-N6 and C5-N6 shows a weak band in the FT-Raman at 1148 cm⁻¹.

Table 3: The selected vibrational wavenumbers (cm⁻¹), measured infrared and Raman band positions (cm⁻¹), and their tentative assignment.

Scaled Wavenumbers (cm ⁻¹)	Experimental Wavenumber (cm ⁻¹)		Intensity		Assignments with PED%
	IR	Raman	IR	Raman	
3446	-	3474 vw	52.13	0.36	v _{ss} N17-H22(100)
3097	-	3198 vw	2.87	0.27	∄ ss C38-H46(92)
3085	-	3106 vw	3.48	0.28	₺ ss C35-H43(99), ₺ ss C52-H51(66)
3071	-	3066 w	4.60	0.47	₽ ss C39-H47(92)
3023	-	3016 w	28.26	0.85	₿ss C41-H44(94)
3009	-	-	31.38	0.35	🕏 as CH2-1 (16), 🗗 as CH2-2(12), 🗗 ss C48-H49(89)
2978	2967 w	2973 s	7.64	0.38	್ರಿ as CH3, ೨ as CH2-1 (41), ೨ as CH2-2(70),
2933	2933 w	-	20.64	0.36	₽ ss CH2-8(82)
2928	2928 s	-	33.74	0.24	₱ss CH3 (45)
2921	2916 s	2922 vs	40.57	0.27	₱ss CH2-3 (64)
2900	-	2875 m	41.93	0.60	₱ss CH2-4 (20),CH2-7(35)
2898	2863 w	2825w	61.16	0.47	₱ss CH2-5 (90),
1677	1650 s	1645 vw	775.72	1.31	∌ ss C=0 (75)
1607	-	1607 vw	0.01	0.58	#ss C35-C36(25), #ss C36-C37(23),#ss C34-C39(20)
1592	-	-	7.32	0.32	#ss C35-C36(17), #ss C37-C38(36), #ss C34-C35(12)
1563	1545 m	1541 m	164.15	0.62	₱ss N21-C16(32), ₱ss C19-C20(37)
1516	-	1511 w	405.07	0.34	₱ss C19-C20(23),ŏsci H22-N17-C16(14)
1487	1483 s	-	25.13	0.91	ðsci CH2-7(80)
1455	-	-	1.10	0.71	ðsci CH2-3(11), ðsci CH2-4(38),ðsci CH2-8(37)
1440	1439 m	1441 m	11.94	0.27	δsci CH2-1(53), δtwi CH3 (20), δsci CH2(8) (81)
1418	-	1403 vw	7.333	0.76	δsci H22-N17-C16(42)
378	1379 s	1378 w	2.76	0.38	τC41-H44-O40-H45(76),δw H22-N17-C16(42)
1361	-	1361 vw	7.0 8	1.80	or CH3(37)
1353	1357 s	-	6.49	0.67	δsci H8-C1-N6(21), τH13-C5-N6-S15(18)
1320	1318 s	-	0.25	0.48	δsci H8-C1-N6(27), τC4-H11-C5-H12(21)
1309	1307 s	1310 w	5.72	0.95	δw H25-C24-C19(29), τ H25-C24-C19-C18(11
1194	1246 vs	-	34.09	7.34	v _s N21-C20(12), 0 ss C19-C24(11), 0 ss C18-C19(10)
1175	-		44.88	0.19	⁵⁵ δsci H32-C31-C34(13), τ H33-C31-C34-C35(15)
1157	-	-	25.58	0.10	ōsci H43-C35-C36(25), ōrH44-C41-O42(21)
1155	-	1148 w	14.86	0.29	₺ ss N6-C1(32), ₺ ss N6-C5(19)
1129	1111 vs	1135 w	86.53	0.11	ϑss N17-C16(14), ϑss N17-C18(21)
1089	-	1087 vw	70.41	0.11	ઝ ss O3-C2(17), ઝ ss C4-C5(17), ઝ ss C1-C2(15)
1071	-	-	14.49	1.59	τ C4-C5-O3-H(11)
1040	1035 s	1036 vw	26.26	0.06	ϑss C24-C27(22), δr CH3(10)

662 — Maha S. Almutairi et al. DE GRUYTER

Continued Table 3: The selected vibrational wavenumbers (cm⁻¹), measured infrared and Raman band positions (cm⁻¹), and their tentative assignment.

Scaled Wavenumbers (cm ⁻¹)	Experimental Wavenumber (cm ⁻¹)		Intensity		Assignments with PED%
	IR	Raman	IR	Raman	
1008	991	1002 vw	4.78	0.16	vss C4-C5(13), vssC1-C2(14)
972	-	-	0.90	0.17	δsci C2-C1-N6(15), τ C4-C5-O3-H(10), τ H13-C5- N6-S15(14)
965	-	954 vw	4.50	1.23	₽ ss C24-C27(18)
909	926 s	907 vw	19.29	0.22	ν _{ss} C24-C27(10), δC34-C39-C38(11)
887	859 s	-	6.12	0.23	δsci N17-C16-N21(12), τ C31-C20-C34-H32(12)
773	788 s	-	36.99	1.61	τ H46-C38-C39-C34(22), τ O23-C19-N17-C18(17)
750	-	736 w	5.91	0.07	τ H25-C24-C19-C18(19), τO23-C19-N17-C8(11),δw CH3(56)
723	722 m	-	11.15	0.04	C37-C36-O40(12), τ C35-C36-C37-C38(10)
681	680 m	685 vw	3.99	0.06	v _{ss} N6-C1(13), v _{ss} S15-N6(20)
575	566 m	568 vw	6.21	0.70	C5-C4-O3(12), τ H22-N17-C18-O23(10), τ C35-C34- C39-C38(21)
552	-	558 vw	10.98	0.09	δr N17-C18-O23(18)
523	-	-	5.39	0.05	δsci C16-N21-C20(38)
488	466 m	-	3.59	0.09	δsci C37-C38-C39(22), ϑss S15-C51(13)
420	-	-	4.86	0.06	δC36-C37-C38(32), δC31-C34-C35(11)
223	-	218 w	0.81	0.59	δC31-C34-C35(11), τ H30-C27-C24-C19(23)
202	-	197 w	3.59	0.26	δC19-C24-C27(12), τ C20-N21-C16-S15(19)
170	-	168 w	1.67	1.00	τ N6-C1-C2-O3(10)
88	-	88 vs	2.81	0.66	τ C5-N6-S15-C16(25)
71	-	70 vs	1.91	0.47	τ C20-N21-C16-N17(15)

v-stretching, δ -bending, τ -Torsion, s-strong, vs-very strong, m-medium, w-weak, vw-very weak, ss-symmetric stretching, as-asymmetric stretching, δ_{sci} -scissoring, δ_{wi} -twisting, δ_{twi} -twist

3.6 HOMO-LUMO energy gap

HOMO and LUMO are called the frontier orbitals since they determine the way the molecule interacts with other species. HOMO is the orbital that could act as an electron donor, since it is the outermost (highest energy) orbital containing electrons, while the LUMO is the orbital that could act as an electron acceptor, since it is the innermost (lowest energy) orbital that has room to accept electrons. A single orbital may be both the HOMO and the LUMO [42]. The lowest singlet transition is the transition from the HOMO orbital to the LUMO orbital [33] and the geometrical relaxation can be understood by analyzing the nodal patterns of the HOMO (-4.15 eV) and LUMO

(-1.55 eV) orbitals with HOMO-LUMO energy gap of 0.2.6 eV for the title compound (Figures 7 and 8). HOMO-LUMO gap is small because the guest atom orbital(s) are only partially occupied and leading to a large stabilization of the LUMO due to the strong electron-accepting ability of the electron-acceptor group. HOMO localizes on the 1,3-benzodioxole moiety and the LUMOs are localized on the pyrimidine ring. Consequently, an ED transfer occurs from the aromatic part of the *p*-conjugated path in the electron-donor side to its electron-withdrawing part. Highly delocalized HOMO indicates that the electrons can more readily move around the molecule and hence an improved intramolecular charge transfer (ICT) [43].

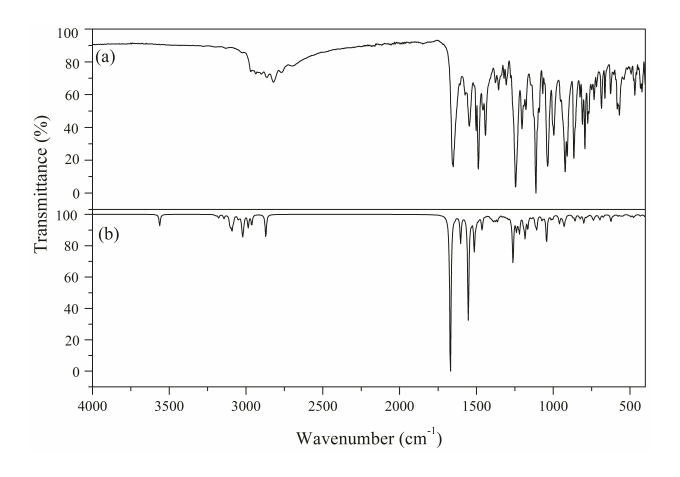


Figure 4: Experimental (a) and simulated (b) IR spectra of the title molecule.

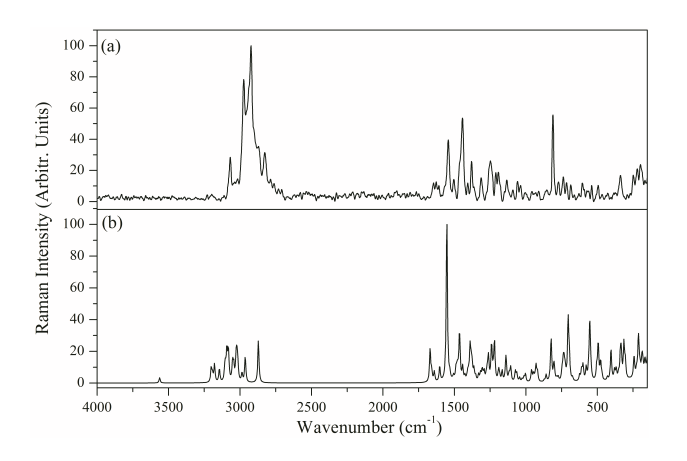


Figure 5: Experimental (a) and simulated (b) Raman spectra of the title molecule.

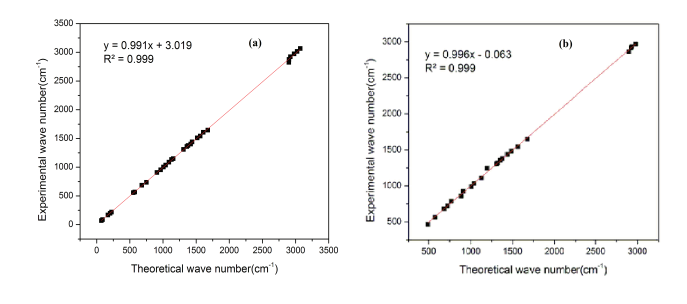


Figure 6: Correlation graphs between theoretical and experimental wavenumbers of (a) FT-IR (b) FT-Raman of the title compound.

3.7 Molecular docking

Molecular docking process involves the prediction of ligand orientation into its targeted binding site [44]. The current study was performed using AutoDock 4.2 program

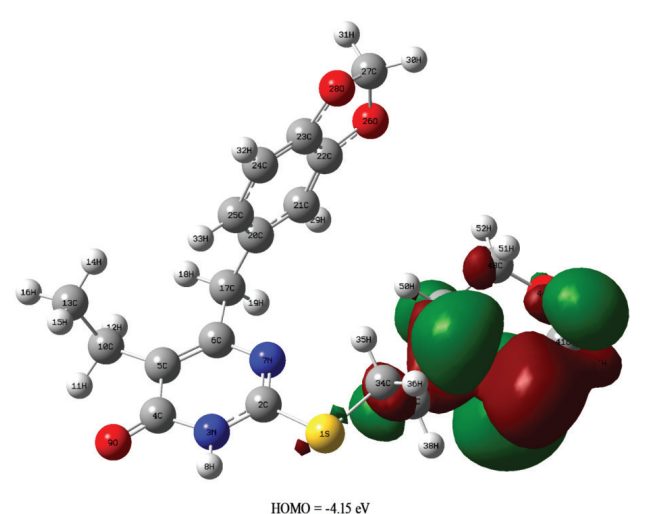
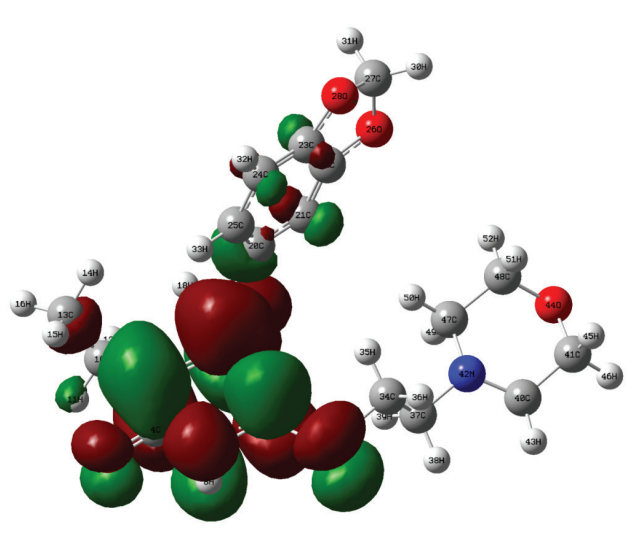


Figure 7: HOMO plot of the title compound.



LUMO = -1.55 eV

Figure 8: LUMO plot of the title compound.

[45]. The title molecule was energy minimized based on the DFT method. Three antimicrobial target proteins with PDB ID: 3QGT (antimalarial) [46], 3ACX and 1VQQ (antibacterial) [47, 48] were selected for the present docking analysis. The three-dimensional structural coordinate files of the target proteins were downloaded from the research collaboratory for structural bioinformatics (RCSB) protein data bank. Grid box size was built 90 x 90 x 90 points as set to be a catalytic site for all target proteins. The binding free energy for interactions of the ligand with proteins 3QGT, 3ACX and 1VQQ are -4.69, -3.94 and -3.29 kcal mol⁻¹, respectively. The best result was obtained with the 3QGT protein for antimalarial activity of the title compound.

Table 4: Molecular docking results with different target proteins.

Target protein ID	Docking energy (kcal.mol ⁻¹)	Atoms of ligands involved in docking	Amino acid residues involved in docking interaction	Bond distance of hydrogen bonds (Å)	No. of hydrogen bonds
3QGT	-4.69	C4-03	ASN66	1.8	2
		C18-023	ARG77	2.5	
ЗАСХ	-3.94	N17-H22	VAL194	1.7	2
		C18-023	LEU189	2.7	
1VQQ	-3.29	N17-H22	SER250	2.0	2
		C4-03	GLU246	2.8	

Fifty conformations of the title molecule were obtained and the top-ranked complex was identified which proved the best fitting. Molecular docking results with different target proteins are shown in Table 4. Pictorial representation of the best possible binding pose of the title compound with 3QGT protein is shown in Figure 9. Docking analysis showed that the carbonyl group in the pyrimidine ring and the oxygen atom of the morpholine group in title compound interact with the ARG77 and ASN66 residues of the target protein, respectively. The title compound forms two hydrogen bonds with ARG77 and ASN66 with distances of 2.5 and 1.8 Å, respectively. The docking results revealed the ability of the title compound for binding to the antibacterial target proteins (3ACX and 1VQQ) and hence it exhibited antimicrobial potential which is consistent with its experimental antimicrobial activity [20]. In addition, prediction of the binding mode of the title compound to the antimalarial target protein (3QGT) was also explored and hence its possible antimalarial potential.

4 Conclusions

A comprehensive FT-IR and FT-Raman spectroscopic investigations as well as DFT computations were carried out on the antimicrobial agent 6-(1,3-benzodioxol-5-ylmethyl)-5-ethyl-2-{[2-(morpholin-4-yl)ethyl]sulfanyl} pyrimidin-4-(3*H*)-one. The geometry optimization of the title molecule exposed its non-planarity. Blue shifting of the C-H wavenumber along with a decrease in bond length of C-H attribute the formation of C-H...O hydrogen bonding. The possibilities of hydrogen bonding were explained with the aid of natural charge analysis. NBO analysis showed a pronounced increase in the lone pair orbital occupancy and hyperconjugation interactions leading to molecular stabilization. HOMO-LUMO energy gap suggested the

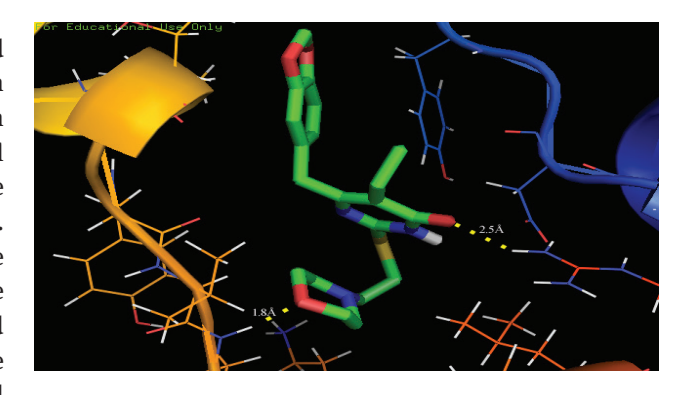


Figure 9: Binding pose diagram of the title compound to its target protein.

possibility of intramolecular charge transfer within the title molecule. Molecular docking results predicted the antimalarial potential of the title compound due to its ability to interact with an antimalarial target protein (3QGT). The results of the current study could support the development of new potent thiouracil-bearing candidates in the antimicrobial research area.

Acknowledgment: The authors would like to extend their sincere appreciation to the Deanship of Scientific Research at King Saud University for its funding of this research through the Research Group Project No. RGP-196.

Conflict of interest: Authors state no conflict of interest.

References

[1] Pałasz A., Cież D., In search of uracil derivatives as bioactive agents. Uracils and fused uracils: Synthesis, biological activity and applications. Eur. J. Med. Chem., 2015, 97, 582-611.

- [2] Al-Deeb O.A., Al-Turkistani A.A., Al-Abdullah E.S., El-Brollosy N.R., Habib E.E., El-Emam A.A., Pyrimidine-5-carbonitrilespart III: synthesis and antimicrobial activity of novel 6-(2-substituted propyl)-2, 4-disubstituted pyrimidine-5carbonitriles. Heterocycl. Commun., 2013, 19, 411-419.
- [3] Conejo-García A., García-Rubiño M.E., Marchal J.A., Núñez M.C., Ramírez A., Cimino S., García M.Á., Aránega A., Gallo M.A., Campos J.M., Synthesis and anticancer activity of (RS)-9-(2,3dihydro-1,4-benzoxaheteroin-2-ylmethyl)-9H-purines. Eur. J. Med. Chem., 2011, 46, 3795-3801.
- [4] López-Cara L.C., Conejo-García A., Marchal J.A., Macchione G., Cruz-López O., Boulaiz H., García M.A., Rodríguez-Serrano F., Ramírez A., Cativiela C., New (RS)-benzoxazepin-purines with antitumour activity: the chiral switch from (RS)-2, 6-dichloro-9-[1-(p-nitrobenzenesulfonyl)-1.2.3.5-tetrahydro-4.1benzoxazepin-3-yl]-9H-purine. Eur. J. Med. Chem., 2011, 46, 249-258.
- [5] Morales F., Ramírez A., Conejo-Garcia A., Morata C., Marchal J.A., Campos J. M., Anti-proliferative activity of 2, 6-dichloro-9-or 7-(ethoxycarbonylmethyl)-9H-or 7H-purines against several human solid tumour cell lines. Eur. J. Med. Chem., 2014, 76, 118-124.
- [6] Parveen H., Hayat F., Salahuddin A., Azam A., Synthesis, characterization and biological evaluation of novel 6-ferrocenyl-4-aryl-2-substituted pyrimidine derivatives. Eur. J. Med. Chem., 2010, 45, 3497-3503.
- [7] Pisal M.M., Nawale L.U., Patil M.D. Bhansali S.G., Gajbhiye J.M., Sarkar D., Chavan S.P., Borate H.B., Hybrids of thienopyrimidinones and thiouracils as anti-tubercular agents: SAR and docking studies. Eur. J. Med. Chem., 2017, 127, 459-469.
- [8] Taher A.T., Abou-Seri S.M., Synthesis and bioactivity evaluation of new 6-aryl-5-cyano thiouracils as potential antimicrobial and anticancer agents. Molecules 2012, 17, 9868-9886.
- [9] Mai A., Rotili D., Massa S., Brosch G., Simonetti G., Passariello C., Palamara A.T., Discovery of uracil-based histone deacetylase inhibitors able to reduce acquired antifungal resistance and trailing growth in Candida albicans. Bioorg. Med. Chem. Lett. 2007, 17, 1221-1225.
- [10] Keche A.P., Hatnapure G.D., Tale R.H., Rodge A.H., Birajdar S.S., Kamble V.M., A novel pyrimidine derivatives with aryl urea, thiourea and sulfonamide moieties: synthesis, antiinflammatory and antimicrobial evaluation. Bioorg. Med. Chem. Lett. 2012, 22, 3445-3448.
- [11] Parker W.B., Enzymology of purine and pyrimidine antimetabolites used in the treatment of cancer. Chem. Rev., 2009, 109, 2880-2893.
- [12] Saladino R., Crestini C., Palamara A.T., Danti M.C., Manetti F., Corelli F., Garaci E., Botta M., Synthesis, biological evaluation, and pharmacophore generation of uracil, 4-(3H)-pyrimidinone, and uridine derivatives as potent and selective inhibitors of parainfluenza 1 (Sendai) virus. J. Med. Chem., 2001, 44, 4554-4562.
- [13] Zhi C., Long Z.-Y., Manikowski A., Brown N.C., Tarantino P.M., Holm K., Dix E.J., Wright G.E., Foster K.A., Butler M.M., Synthesis and antibacterial activity of 3-substituted-6-(3-ethyl-4-methylanilino) uracils. J. Med. Chem., 2005, 48, 7063-7074.
- [14] Leite A.C.L., da Silva K.P., de Souza I.A., de Araújo J.M., Brondani D.J., Synthesis, antitumour and antimicrobial activities of new peptidyl derivatives containing the

- 1,3-benzodioxole system. Eur. J. Med. Chem., 2004, 39, 1059-
- [15] Joshi R., Kumar M.S., Satyamoorthy K., Unnikrisnan M., Mukherjee T., Free radical reactions and antioxidant activities of sesamol: pulse radiolytic and biochemical studies. J. Agric. Food Chem., 2005, 53, 2696-2703.
- [16] Cotinguiba F., Regasini L.O., da Silva Bolzani V., Debonsi H.M., Passerini G.D., Cicarelli R.M.B., Kato M.J., Furlan M., Piperamides and their derivatives as potential antitrypanosomal agents. Med. Chem. Res., 2009, 18, 703.
- [17] Bezerra D.P., Castro F.O. D., Alves A.P.N., Pessoa C., Moraes M.O.D., Silveira E.R., Lima M.A.S., Elmiro F.J.M., Alencar N., Mesquita R.O., In vitro and in vivo antitumor effect of 5-FU combined with piplartine and piperine. J. Appl. Toxicol., 2008, 28, 156-163.
- [18] Viegas-Junior C., Danuello A., da Silva Bolzani V., Barreiro E.J., Fraga C.A.M., Molecular hybridization: a useful tool in the design of new drug prototypes. Curr. Med. Chem., 2007, 14, 1829-1852.
- [19] Tietze L.F., Bell H.P., Chandrasekhar S., Natural product hybrids as new leads for drug discovery. Angew. Chem. Int. Ed. 2003, 42, 3996-4028.
- [20] Attia M.I., El-Brollosy N.R., Kansoh A.L., Ghabbour H.A., Al-Wabli R.I. Fun H.-K., Synthesis, Single crystal x-ray structure, and antimicrobial activity of 6-(1, 3-benzodioxol-5-ylmethyl)-5ethyl-2-{[2-(morpholin-4-yl)ethyl]sulfanyl}pyrimidin-4 (3H)-one. J. Chem., 2014, 2014, Article ID 457430.
- [21] Frisch MJ, Trucks GW, Schlegel HB, Scuseria GE, Robb MA, Cheeseman JR, Scalmani G, Barone V, Mennucci B, Petersson GA, Nakatsuji H, Caricato M, Li X, Hratchian HP, Izmaylov AF, Bloino J, Zheng G, Sonnenberg JL, Hada M, Ehara M, Toyota K, Fukuda R, Hasegawa J, Ishida M, Nakajima T, Honda Y, Kitao O, Nakai H, Vreven T, Montgomery Jr JA, Peralta JE, Ogliaro F, Bearpark M, Heyd JJ, Brothers E, Kudin KN, Staroverov VN, Kobayashi R, Normand J, Raghavachari K, Rendell A, Burant JC, Iyengar SS, Tomasi J, Cossi M, Rega N, Millam JM, Klene M, Knox JE, Cross JB, Bakken V, Adamo C, Jaramillo J, Gomperts R, Stratmann RE, Yazyev O, Austin AJ, Cammi R, Pomelli C, Ochterski JW, Martin RL, Morokuma K, Zakrzewski VG, Voth GA, Salvador P, Dannenberg JJ, Dapprich S, Daniels AD, Farkas O, Foresman JB, Ortiz JV, Cioslowski J, Fox DJ, Gaussian-09, Revision A.02, Gaussian, Inc., Wallingford CT, 2009.
- [22] Lee C., Yang W., Parr R.G., Development of the Colle-Salvetti correlation-energy formula into a functional of the electron density. Phys. Rev. B, 1988, 37, 785.
- [23] Becke A.D., Density-functional thermochemistry. IV. A new dynamical correlation functional and implications for exactexchange mixing. J. Chem. Phys., 1996, 104, 1040-1046.
- [24] Almutairi M.S., Muthu S., Prasana J.C., Chandralekha B., Al-Ghamdi A.R., Attia M. I. Comprehensive spectroscopic (FT-IR, FT-Raman, ¹H and ¹³C NMR) identification and computational studies on 1-acetyl-1H-indole-2,3-dione. Open Chem., 2017, 15, 225-237.
- [25] Al-Wabli R.I., Govindarajan M., Almutairi M.S., Attia M.I. A combined experimental and theoretical study on vibrational and electronic properties of (5-methoxy-1H-indol-1-yl) (5-methoxy-1H-indol-2-yl)methanone. Open Chem., 2017, 15, 238-246.

- [26] Scott A.P., Radom L., Harmonic vibrational frequencies: an evaluation of Hartree– Fock, Møller– Plesset, quadratic configuration interaction, density functional theory, and semiempirical scale factors. J. Phys. Chem. 1996, 100, 16502-16513.
- [27] Jamróz M.H., Vibrational energy distribution analysis (VEDA): scopes and limitations. Spectrochim. Acta A Mol. Biomol. Spectrosc., 2013, 114, 220-230.
- [28] Keresztury G., Raman Spectroscopy: Theory in: JM Chalmers, PR Griffiths (Ed.), Hand book of vibrational spectroscopy, vol. 1. Wiley: 2002.
- [29] Attia M.I., Kansoh A.L., El-Brollosy N.R., Antimicrobial pyrimidinones II: synthesis and antimicrobial evaluation of certain novel 5, 6-disubstituted 2-(substituted amino) alkylthiopyrimidin-4(3H)-ones. Monatsh. Chem.-Chem. Mon. 2014, 145, 1825-1837.
- [30] Amalanathan M., Rastogi V., Joe I.H., Palafox M., Tomar R., Density functional theory calculations and vibrational spectral analysis of 3, 5-(dinitrobenzoic acid). Spectrochim. Acta A Mol. Biomol. Spectrosc., 2011, 78, 1437-1444.
- [31] Edwin B., Amalanathan M., Joe I.H., Vibrational spectra and natural bond orbital analysis of organic crystal L-prolinium picrate. Spectrochim. Acta A Mol. Biomol. Spectrosc., 2012, 96, 10-17.
- [32] Reed A.E., Curtiss L.A., Weinhold F., Intermolecular interactions from a natural bond orbital, donor-acceptor viewpoint. Chem. Rev., 1988, 88, 899-926.
- [33] Xavier T., Rashid N., Joe I.H., Vibrational spectra and DFT study of anticancer active molecule 2-(4-bromophenyl)-1*H*-benzimidazole by normal coordinate analysis. Spectrochim. Acta A Mol. Biomol. Spectrosc., 2011, 78, 319-326.
- [34] Benzon K., Varghese H.T., Panicker C.Y., Pradhan K., Tiwary B.K., Nanda A.K. Van Alsenoy C., Spectroscopic and theoretical characterization of 2-(4-methoxyphenyl)-4, 5-dimethyl-1*H*-imidazole 3-oxide. Spectrochim. Acta A Mol. Biomol. Spectrosc., 2015, 151, 965-979.
- [35] Mulliken R.S., Electronic population analysis on LCAO-MO molecular wave functions. I. J. Chem. Phys., 1955, 23, 1833-1840
- [36] Gussoni M., Castiglioni C., Ramos M.N., Rui M., Zerbi G., Infrared intensities: from intensity parameters to an overall understanding of the spectrum. J. Mol. Struct., 1990, 224, 445-470.
- [37] King W., Mast G., Blanchette P., Infrared intensity sum rule and effective charges. J. Chem. Phys., 1972, 56, 4440-4446.
- [38] Benzon K., Varghese H.T., Panicker C.Y., Pradhan K., Tiwary B.K., Nanda A.K., Van Alsenoy C., Spectroscopic investigation (FT-IR and FT-Raman), vibrational assignments, HOMO–LUMO, NBO, MEP analysis and molecular docking study of 2-(4-hydroxyphenyl)-4, 5-dimethyl-1*H*-imidazole 3-oxide. Spectrochim. Acta A Mol. Biomol. Spectrosc., 2015, 146, 307-322.

- [39] Lin-Vien D., Colthup, N.B., Fateley W.G., Grasselli J.G., The handbook of infrared and Raman characteristic frequencies of organic molecules, Elsevier: 1991.
- [40] Smith B.C., Infrared spectral interpretation: a systematic approach, CRC press, 1998.
- [41] Kaur M., Mary Y.S., Panicker C.Y., Varghese H.T., Yathirajan H., Byrappa K., Van Alsenoy C., Vibrational spectroscopic (FT-IR, FT-Raman) and quantum chemical calculations of 1-(5, 5-dioxido-10H-phenothiazin-10-yl) ethanone. Spectrochim. Acta A Mol. Biomol. Spectrosc., 2014, 120, 445-455.
- [42] Joe I.H., FT-IR, Raman and DFT study of 2-amino-5-fluorobenzoic acid and its biological activity with other halogen (Cl, Br) substitution. Spectrochim. Acta A Mol. Biomol. Spectrosc., 2011, 79, (2), 332-337.
- [43] Atalay Y., Avcı D., Başoğlu A., Linear and non-linear optical properties of some donor-acceptor oxadiazoles by ab initio Hartree-Fock calculations. Struct. Chem. 2008, 19, 239-246.
- [44] Kitchen D.B., Decornez H., Furr J.R., Bajorath J., Docking and scoring in virtual screening for drug discovery: methods and applications. Nat. Rev. Drug Discov., 2004, 3, 935-949.
- [45] Morris G.M., Huey R., Lindstrom W., Sanner M.F., Belew R.K., Goodsell D.S., Olson A.J., AutoDock4 and AutoDockTools4: Automated docking with selective receptor flexibility. J. Comput. Chem., 2009, 30, 2785-2791.
- [46] Kamchonwongpaisan S., Quarrell R., Charoensetakul N., Ponsinet R., Vilaivan T., Vanichtanankul J., Tarnchompoo B., Sirawaraporn W., Lowe G., Yuthavong Y., Inhibitors of multiple mutants of Plasmodium f alciparum dihydrofolate reductase and their antimalarial activities. J. Med. Chem. 2004, 47, 673-680.
- [47] Kotaiah Y., Nagaraju K., Harikrishna N., Rao C.V., Yamini L., Vijjulatha M., Synthesis, docking and evaluation of antioxidant and antimicrobial activities of novel 1,2,4-triazolo[3,4-b][1,3,4] thiadiazol-6-yl)selenopheno[2,3-d]pyrimidines. Eur. J. Med. Chem., 2014, 75, 195-202.
- [48] Acebrón I., Chang M., Mobashery S.; A Hermoso J., The allosteric site for the nascent cell wall in penicillin-binding protein 2a: an Achilles' heel of methicillin-resistant Staphylococcus aureus. Curr. Med. Chem. 2015, 22, 1678-1686.